




Enhanced multichannel dual-comb spectroscopy of complex systems

Razmik Aramyan ^{*}, Oleg Tretiak , and Sushree S. Sahoo 

*Johannes Gutenberg-Universität Mainz, 55128 Mainz, Germany and
Helmholtz-Institut Mainz, GSI Helmholtzzentrum für Schwerionenforschung, 55128 Mainz, Germany*

Dmitry Budker 

*Johannes Gutenberg-Universität Mainz, 55128 Mainz, Germany
Helmholtz-Institut Mainz, GSI Helmholtzzentrum für Schwerionenforschung, 55128 Mainz, Germany and
Department of Physics, University of California, Berkeley, CA 94720, USA*

(Dated: March 14, 2025)

A multichannel dual-comb spectroscopy (DCS) approach for high-resolution, broadband spectral measurements is presented, demonstrating its effectiveness in studying complex atomic systems. By implementing a photodetector array, we enhance DCS capabilities, addressing the fundamental trade-off between signal-to-noise ratio (SNR) and spectral coverage. To resolve ambiguities in frequency conversion, we introduced a relative offset in beat note frequency, ensuring accurate spectral reconstruction. As a proof of concept, the absorption spectrum of samarium (Sm) vapor is investigated over a 52 nm range, and several previously unreported absorption lines are detected. This is a step toward “Spectroscopy 2.0”, enabling massively parallel spectroscopic measurements (including those at >100 T magnetic fields) crucial for atomic physics and fundamental interactions research.

I. INTRODUCTION

A diverse selection of atomic systems with a range of properties is essential for optimizing sensitivity to specific interactions of interest in fundamental physics experiments. This need is particularly pressing in the rapidly expanding field of searches for new physics using atoms and molecules [1]. While atomic databases provide valuable spectral information [2], their coverage remains incomplete, especially for rare-earth and actinide elements. The primary reason for these gaps in atomic tables is the complexity of dense atomic spectra, which present significant challenges for both experimental measurements and theoretical modeling. In ref. [3], a novel approach to spectroscopy (called Spectroscopy 2.0) is introduced, integrating three key elements: (1) massively parallel spectroscopic tool, (2) tunable high magnetic fields that introduce a new spectroscopic dimension, and (3) advanced many-body theory enhanced by modern computational power and machine learning.

In this paper, we take the first step toward implementing Spectroscopy 2.0: development of a massively parallel spectroscopic tool. As the core technique, we employ dual-comb spectroscopy (DCS), a revolutionary method renowned for its high-resolution, high-sensitivity, and broadband spectral measurements at remarkable speed [4–7].

The two optical frequency combs used for DCS typically have repetition rates on the order of hundreds of megahertz, differing from each other

by hundreds of hertz. The beat signal between the two combs is in itself a frequency comb but now in the radio frequency (RF) domain. Each line of this comb contains information about its “parent” pair of optical frequencies. Detecting beat signals on a photodetector allows one to obtain information about the optical domain, enabling direct measurement of complex spectra, for example complex molecular spectra in the near-infrared (NIR) range [8, 9].

While DCS enables high-speed measurements within a broad wavelength range, its performance is fundamentally limited by the inability to detect weak signals at each beat note frequency. In our frequency comb system, a few hundred milliwatts of total output light power is distributed across a broad spectrum (from 650 nm to 2100 nm), often resulting in hundreds-of-nanowatt-level power per comb tooth. Detecting these weak signals with high precision requires a detection system that combines high sensitivity, broadband coverage, and a wide dynamic range capabilities that are challenging to achieve with traditional single-element detectors.

A PIN photodiode, for example, can handle the high total power of a broad band comb light due to its large linear dynamic range and robustness. However, it lacks internal gain, which makes it poorly suited for resolving individual beat notes. When the total comb light is incident on a PIN photodiode, the weak beat note signals of individual comb teeth are masked by the noise floor, which includes contributions from shot noise, diode dark current, Johnson noise, etc. As a result, the signal-to-noise ratio (SNR) for individual beat note frequencies becomes insufficient for precise measurements [10].

However, light-noise-limited dual-comb spec-

^{*} Contact author: aramyanr@uni-mainz.de

troscopy can be achieved using detectors with intrinsic amplification, such as avalanche photodiodes (APDs), photomultiplier tubes, or hybrid detectors. These detectors are capable of sensing low light levels down to a single photon. However, they cannot handle high-intensity total light. In the papers [11, 12], light-noise-limited dual-comb spectroscopy was achieved using single-photon detectors and by limiting the optical bandwidth.

In our work, we aimed to achieve light-noise-limited detection while simultaneously measuring a broadband optical spectrum (several tens of nanometers). As proposed in Ref. [10], in a light-noise-limited condition, the use of multiple photodetectors enhances SNR. Spectrally dispersing the comb light across an array of APDs leads to several key advantages:

- **Optimized Dynamic Range:** By limiting the input power to each APD by narrowing spectral slice, we avoid saturation and maintain linear operation, ensuring accurate and reliable measurements.
- **Improved Signal-to-Noise Ratio (SNR):** The combination of high gain and spectral filtering results in a significantly improved SNR for individual beat notes.
- **Broadband Coverage:** The array collectively covers 52 nm; the coverage can potentially be broadened even further.

This approach opens up the possibility of performing broadband DCS with a high SNR. However, in previous works, another limitation of DCS has been mentioned [7, 13]. The maximum optical range that can be acquired without aliasing when the repetition rates are fixed is usually defined as

$$\Delta\nu = \frac{f_r^2}{2\delta f_r}, \quad (1)$$

where f_r denotes the repetition rate of one of the frequency combs and δf_r is the difference in repetition rates between the two combs. When the recorded optical range exceeds $\Delta\nu$, the beat notes of the optical frequencies begin to alias each other, leading to ambiguity in the interpretation of the data. This problem can be solved by selecting the repetition rates of the combs such that $k(f_{r1,2}/2)/\delta f_r$ is not an integer, where $k = 1, 2, 3, \dots$ which introduces a relative offset between overlapping RF combs and acquiring data with high enough resolution.

In this work, we demonstrate ambiguity-free, broadband spectroscopy ($\Delta\lambda \approx 52$ nm) of samarium (Sm, atomic number $Z=62$) with a high SNR (≈ 900). This enables the detection of several unreported transitions.

II. AMBIGUITY IN FREQUENCY CONVERSION

The beat signal between the two combs, acquired by a photodetector, contains radio frequencies, and to retrieve the corresponding optical frequencies, we must convert this RF spectrum back into optical domain. A visual representation of this frequency mapping, Fig. 1(a), can help to understand the conversion process. To ensure that only the beat note between neighboring optical lines is acquired, the maximum frequency in the RF domain (the vertical axis) should be limited to $\leq f_r/2$. The values $i\Delta\nu$, (where $i = 0, 1, 2, \dots$ and $\Delta\nu$ is defined in Eq. (1)) delimit i th unambiguity region on the horizontal axis. The black vertical dashed lines denote the optical frequency ranges captured by each photodiode, whereas the horizontal dashed lines represent the RF frequencies of the corresponding recorded signals. To convert the RF spectrum we should start with the general representation of the optical frequencies of the comb:

$$\begin{aligned} \nu_{1n} &= f_{\text{CEO1}} + n f_{r1}, \\ \nu_{2m} &= f_{\text{CEO2}} + m f_{r2}, \end{aligned} \quad (2)$$

where n and m represent the tooth numbers of corresponding optical frequencies ν_{1n} and ν_{2m} of the first and second comb, respectively, and $f_{\text{CEO1,2}}$ is the carrier-envelope offset. In our case, we lock the system such that $f_{\text{CEO1}} = f_{\text{CEO2}}$.

Since both combs contribute equally to each beat note, it is necessary to select one of them to serve as a reference for our calculation frame. We will choose the comb with the smaller repetition rate (this is an arbitrary choice); let us consider $f_{r1} < f_{r2}$. The beat note (f_{RF}) between pair of teeth is:

$$f_{\text{RF}} = |\nu_{1n} - \nu_{2m}| = |n f_{r1} - m f_{r2}|. \quad (3)$$

The relationship between n and m for neighboring teeth depends on the number of $f_{r1}/2$ border crossings (j) up to that region, such that $n = m - j$. By comparing these RF frequencies with the recorded ones, we can reconstruct the corresponding optical frequencies. However, to use this technique, we must ensure that the f_{RF} from different regions are unambiguously distinguished. An ambiguity would occur when $k(f_{r1}/2)/\delta f_r$ is an integer, where $k = 1, 2, 3, \dots$. As shown in Fig. 1(a), channel 4 contains signals from two different regions and hence exhibits ambiguity, while other channels such as channel 2 remain unambiguous. In an experiment, an additional complication may arise due to cross-talk between photodiodes.

We propose to resolve the ambiguity in the following manner: when $k(f_{r1}/2)/\delta f_r$ is not an integer, RF combs from different regions will exhibit

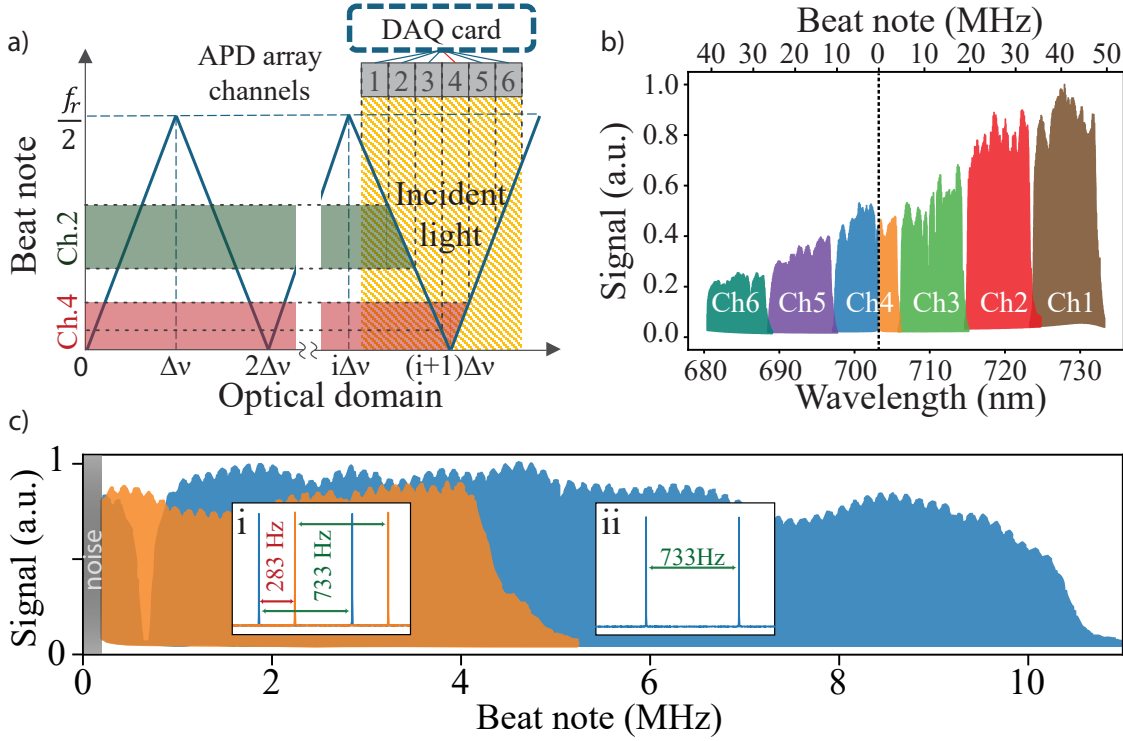


Figure 1. Mapping of the incident light frequencies to the RF frequencies: a) The general mapping method, with an example of ambiguous and unambiguous data. Channel 2 (unambiguous data) and channel 4 (ambiguous data) are labeled as Ch. 2 and Ch. 4, respectively. b) The real data from six channels illustrates the signal along with its recorded RF frequencies and corresponding wavelengths. This data represents Sm spectrum at 1040°C . c) The normalized recorded spectrum on channel 4, where ambiguity is expected (for $\delta f_r \approx 733\text{ Hz}$). The blue and orange data represent spectra from different unambiguous regions. These components were separated during the data analysis process. As illustrated in the two smaller zoomed-in figures when the two spectra overlap (i), we observe two sets of teeth with a relative offset of 283 Hz, whereas in case of no ambiguity, we see only one set of teeth with a 733 Hz spacing (ii). Moreover in the overlapping region, a dip in the blue spectra corresponds to a strong absorption line of samarium.

a relative offset. This offset can be observed if the acquisition time is longer than the inverse of relative offset or, in other words, spectral resolution is better than relative offset. The relative offset can be determined by comparing simulated RF combs from different regions of unambiguity with each other.

In Fig. 1(b), we present the data acquired with our system. The expected ambiguity in the spectrum as recorded in channel 4 is shown in Fig. 1(c). In this case, $\delta f_r \approx 733.04\text{ Hz}$, so if aliasing were present, there would be only teeth separated by δf_r . However, we observe two sets of comb lines with a relative offset of 283 Hz in the overlapping region of the spectra as shown in the inset (i) of Fig. 1(c). “Unfolding” the data as described above allows us to attribute the spectral peaks to their correct optical frequencies.

One can resolve this ambiguity by aligning the system so that the crossing occurs exactly between two channels. However, when multiple crossings occur across the spectrum, it becomes difficult to tune the system in a way that ensures

none of the photodiodes exhibit ambiguity. Instead, addressing these ambiguities during post-analysis using the method described above is significantly easier and more practical.

III. EXPERIMENTAL SETUP

The experimental setup (Fig. 2) incorporates a pair of MenloSystems FC1500-250-ULN combs locked to a low phase noise, narrow linewidth ($< 1\text{ kHz}$) 1542 nm laser diode (RIO Planex). Then, the repetition rate of each comb follows the laser diode frequency and is stabilized to an FS725 rubidium frequency standard (Stanford Research Systems) via the laser diode. The system generates femtosecond pulses with repetition rates $\approx 250\text{ MHz}$ ($f_{r1} \approx 250000240.75\text{ Hz}$ and $f_{r2} \approx 250000973.79\text{ Hz}$) and covers a spectral range from 650 nm to 2100 nm. The outputs of the two combs are combined using a beam splitter and passed through a samarium (Sm) cell maintained at a temperature of $\approx 1040^\circ\text{C}$ to produce

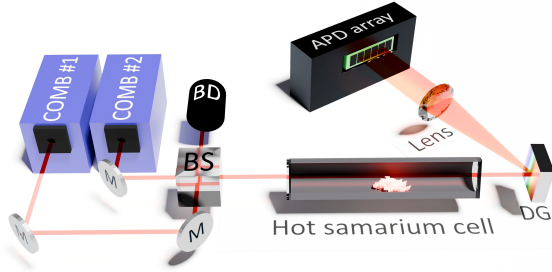


Figure 2. Schematic of the experimental setup, where M: mirror, BS: beam splitter, BD: beam dump and DG: diffraction grating.

a sufficient density of Sm atoms at a buffer gas (argon) pressure of 330 torr. At the temperature and pressure used, the combined Doppler and collisionally broadened linewidth of atomic transitions (on the order of a gigahertz) is sufficiently large, so that several comb teeth (≈ 250 MHz separation defined by the pulse repetition rate) fall under the line profile. The combined light beam is spectrally dispersed with a grating onto the avalanche photodiode (APD) array.

The APD array used in this experiment is Hamamatsu S15249. It consists of 1×16 diodes with separate output channels of uniform gain. In this work, only six of them were used as a proof of principle. The array has a spectral response range of 350–1000 nm, with peak sensitivity at 620 nm. We equip each APD channel with a dedicated transimpedance amplifier with a 125 MHz bandwidth, placed as close as possible to the APD array chip, and allowing simultaneous operation across all channels. The common cathode was powered by a linear voltage-stabilized power supply, ensuring low-noise performance, particularly at high frequencies (> 50 Hz). The APD of bias voltage was adjusted to optimize the APD gain and achieve the best possible SNR. This choice is motivated by the low output power of the laser in the visible range, where it is critical to ensure that the background noise of the photodetector remains smaller than the laser light noise.

In this work, we used the same acquisition system as described for “Apparatus A” in [14]. Specifically, we used a two-channel digitizer (Spectrum M4i.4420-x8) with a 250 MHz sampling rate and 16-bit resolution. The digitizers clock frequency was locked to the same rubidium frequency standard as the combs.

The system captures spectra up to 125 MHz (the Nyquist frequency) with a resolution of 0.93 Hz. Data were recorded in chunks of 2^{28} samples per channel (≈ 1.073 s of data) and Fourier-transformed on a graphics card in parallel, ensuring continuous acquisition without interruptions. For simplicity, we call it a “one-second” data record. In this work, we did not apply any

special window function to the data (a rectangular window was used). The resulting spectra were averaged using the central processor. For details on the data acquisition system, refer to the supplementary materials [14].

The system imposes no restrictions on the number of spectra that can be averaged. In our experiment, we averaged 1000 spectra per measurement (≈ 17 min). Data from both channels were collected simultaneously. Since the system operates in parallel and each channel functions independently, the number of computers with digitizers can be scaled to enable simultaneous recording across any number of channels. The independent systems can be synchronized using an external trigger.

The high spectral resolution reveals a scalloping pattern between the acquisition system and the RF comb. Various methods can mitigate these artifacts during post-analysis. Our approach involves detecting the peaks of the teeth in the recorded spectrum and redistributing the energy of neighboring bins of the tooth.

IV. RESULTS

The incident light had an optical bandwidth of ≈ 9 nm on each photodiode. As our acquisition system has only two parallel data channels, we performed three sets of two-channel acquisitions (parallel channels: 1&2 | 3&4 | 5&6), covering a total optical range of ≈ 52 nm (680 nm to 732 nm) shown in Fig.1(b). To maintain a high SNR we averaged 1000 one-second recordings. The SNR varies across the spectrum due to intensity change, as the recorded spectrum lies on the edge of the emission spectrum of the combs. The average SNR is ≈ 900 , the SNR was calculated as follows:

$$SNR = \frac{\sqrt{Tooth\ Height^2 - Baseline^2}}{\sigma}, \quad (4)$$

where σ is the standard deviation of the points between two teeth. This approach achieves a DCS figure of merit of $M \times SNR / \sqrt{\tau} = 3.5 \times 10^6 \text{ Hz}^{1/2}$, and constrained only by the number of the used elements of the photodetector array. In Fig. 3, the most interesting spectrum of the six channels is presented, showing several absorption lines. The high-resolution plots of this spectrum and the remaining channels can be found in the supplementary materials. We compared measurements taken at different cell temperatures, $\approx 530^\circ\text{C}$ and $\approx 1040^\circ\text{C}$, to analyze spectral variations at low and high samarium concentrations. These data can also be used to normalize the etalon effect caused by optical elements, which appear as oscillations in the spectrum.

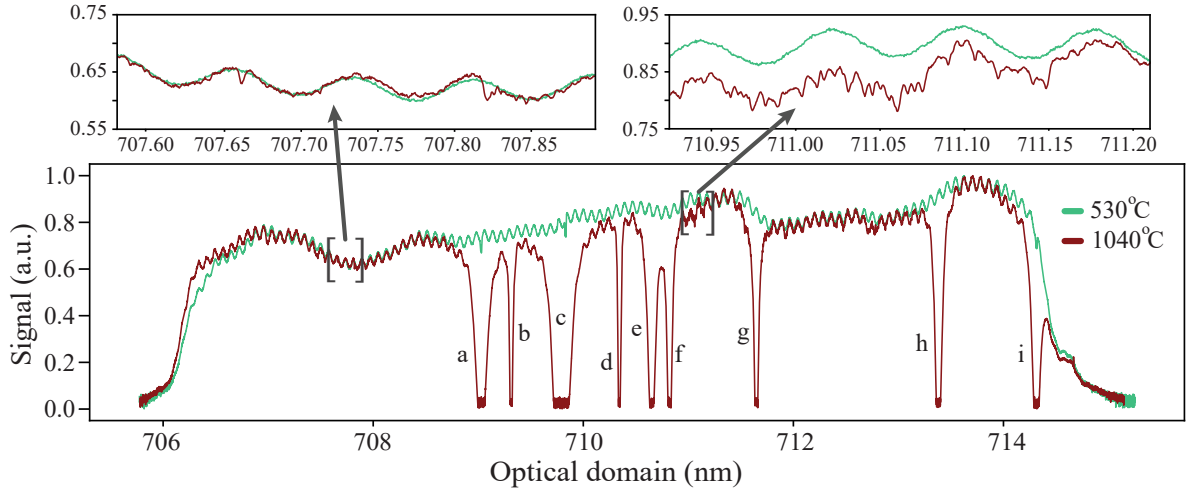


Figure 3. Absorption spectrum of Sm vapor at various temperatures, obtained by averaging 1000 spectra of one-second records on channel 3, resulting in an SNR of 1100. The smaller plots show zoomed-in regions where several unknown lines have been detected. The numerical values of the wavelengths for strong transitions are: a - 709.030 nm, b - 709.314 nm, c - 709.828 nm, d - 710.343 nm, e - 710.653 nm, f - 710.823 nm, g - 711.648 nm, h - 713.383 nm, and i - 714.316 nm

When compared with the existing dataset [15–17], numerous previously unknown lines were detected. Two zoomed-in subplots illustrate spectral regions with sparse and dense transition lines. To ensure that dense spectral regions are not misinterpreted as system noise, the data at $\approx 530^\circ\text{C}$ is provided, demonstrating that the noise level remains consistent across different spectral regions. The detected unknown transitions require further investigation for proper characterization.

V. CONCLUSION

We present a successful enhancement of the DCS technique by incorporating a photodetector array, effectively addressing the trade-off between SNR and optical bandwidth. It also demonstrates the capability of this technique to acquire a broad spectrum without ambiguity, by introducing a relative offset to RF comb tooth sets from different unambiguity regions. By acquiring data with high spectral resolution, we were able to resolve and reconstruct the unambiguous spectrum. Furthermore, this approach enabled the detec-

tion of numerous previously unreported transition lines, highlighting its potential for discovering new spectral features.

The ability of this system to acquire spectra with both broad bandwidth and high SNR makes it a valuable tool for Spectroscopy 2.0. The next step of this project is to design and implement experiments at high magnetic field environments, up to the 100T [18, 19], to explore the effects of strong fields on atomic transitions.

VI. ACKNOWLEDGEMENT

The authors thank Nathalie Picqué, Jason Stalnaker, Arman Cingöz, and Mikhail Kozlov for helpful discussions. This work was supported by the European Commission Horizon Europe Framework Program under the Research and Innovation Action MUQUABIS GA no. 101070546.

VII. DATA AVAILABILITY

The data supporting the plots in this article and the supplementary plots are available from the corresponding author upon request.

-
- [1] M. Safronova, D. Budker, D. DeMille, D. F. J. Kimball, A. Derevianko, and C. W. Clark, Search for new physics with atoms and molecules, *Reviews of Modern Physics* **90**, 025008 (2018).
 - [2] A. Kramida and Y. Ralchenko, *Nist atomic spectra database, nist standard reference database 78*.

- [3] R. Battesti, J. Beard, S. Bser, N. Bruyant, D. Budker, S. A. Crooker, E. J. Daw, V. V. Flambaum, T. Inada, I. G. Irastorza, F. Karbstein, D. L. Kim, M. G. Kozlov, Z. Melhem, A. Phipps, P. Pognat, G. Rikken, C. Rizzo, M. Schott, Y. K. Semertzidis, H. H. ten Kate, and G. Zavattini, High magnetic fields for fundamental physics, *Physics Reports* **765766**, 1

- (2018).
- [4] T. W. Hänsch, Nobel lecture: Passion for precision, *Reviews of Modern Physics* **78**, 1297 (2006).
 - [5] S. Schiller, Spectrometry with frequency combs, *Optics Letters* **27**, 766 (2002).
 - [6] N. Picqué and T. W. Hänsch, Frequency comb spectroscopy, *Nature Photonics* **13**, 146 (2019).
 - [7] I. Coddington, N. Newbury, and W. Swann, Dual-comb spectroscopy, *Optica* **3**, 414 (2016).
 - [8] E. Baumann, F. R. Giorgetta, W. C. Swann, A. M. Zolot, I. Coddington, and N. R. Newbury, Spectroscopy of the methane ν_3 band with an accurate midinfrared coherent dual-comb spectrometer, *Physical Review A* **84**, 062513 (2011).
 - [9] Z. Wei, X. Ren, M. Yan, and H. Zeng, The development and application of dual-comb spectroscopy in analytical chemistry, *Chinese Chemical Letters* **34**, 107254 (2023).
 - [10] N. R. Newbury, I. Coddington, and W. Swann, Sensitivity of coherent dual-comb spectroscopy, *Optics Express* **18**, 7929 (2010).
 - [11] B. Xu, Z. Chen, T. W. Hänsch, and N. Picqué, Near-ultraviolet photon-counting dual-comb spectroscopy, *Nature* **627**, 289 (2024).
 - [12] N. Picqué and T. W. Hänsch, Photon-level broadband spectroscopy and interferometry with two frequency combs, *Proceedings of the National Academy of Sciences* **117**, 26688 (2020).
 - [13] Y. Sugiyama, T. Kashimura, K. Kashimoto, D. Akamatsu, and F.-L. Hong, Precision dual-comb spectroscopy using wavelength-converted frequency combs with low repetition rates, *Scientific Reports* **13**, 10.1038/s41598-023-29734-2 (2023).
 - [14] O. Tretiak, X. Zhang, N. L. Figueroa, D. Antypas, A. Brogna, A. Banerjee, G. Perez, and D. Budker, Improved bounds on ultralight scalar dark matter in the radio-frequency range, *Phys. Rev. Lett.* **129**, 031301 (2022).
 - [15] C. Ferrara, M. Giarrusso, and F. Leone, Experimental atomic data of spectral lines - I. Cs, Ba, Pr, Nd, Sm, Eu, Gd, Tb, Dy, Ho, Er, Tm, Yb, Lu, Hf, Re, and Os in the 370-1000nm interval, *Monthly Notices of the Royal Astronomical Society* **527**, 4440 (2023).
 - [16] W. Martin, R. Zalubas, and L. Hagan, *Atomic Energy Levels - The Rare-Earth Elements: The Spectra of Lanthanum, Cerium, Praseodymium, Neodymium, Promethium, Samarium, Europium, Gadolinium, Terbium, Dysprosium, Holmium, Erbium, Thulium, Ytterbium, and Lutetium* (National Bureau of Standards, 1978).
 - [17] W. F. Meggers, C. H. Corliss, and B. F. Scribner, *Tables of spectral-line intensities: part 1-arranged by elements* (National Bureau of Standards, 1975).
 - [18] B. Hervieu, C. Berriaud, R. Berthier, F. Debray, P. Fazilleau, P. Manil, M. Massinger, R. Pfister, P. Pognat, L. Ronayette, and C. Trophime, Cryogenic design of the 43 T LNCMI Grenoble hybrid magnet, *Physics Procedia* **67**, 692 (2015).
 - [19] J. Beard, J. Billette, N. Ferreira, P. Frings, J.-M. Lagarrigue, F. Lecouturier, and J.-P. Nicolin, Design and tests of the 100-T triple coil at LNCMI, *IEEE Transactions on Applied Superconductivity* **28**, 1 (2018).